Available online at www.sciencedirect.com
SCIENCE DIRECT
Journal of Sound and Vibration 293 (2006) 611–625
JOURNAL OF SOUND AND VIBRATION
www.elsevier.com/locate/jsvi

Coupled boundary and finite element analysis of vibration from railway tunnels—a comparison of two- and three-dimensional models

L. Andersen[a,*], C.J.C. Jones[b]

[a]*Department of Civil Engineering, Aalborg University, Denmark*
[b]*Institute of Sound and Vibration Research, University of Southampton, UK*

Accepted 26 August 2005
Available online 19 January 2006

Abstract

The analysis of vibration from railway tunnels is of growing interest as new and higher-speed railways are built under the ground to address the transport problems of growing modern urban areas. Such analysis can be carried out using numerical methods but models and therefore computing times can be large. There is a need to be able to apply very fast calculations that can be used in tunnel design and studies of environmental impacts. Taking advantage of the fact that tunnels often have a two-dimensional geometry in the sense that the cross section is constant along the tunnel axis, it is useful to evaluate the potential uses of two-dimensional models before committing to much more costly three-dimensional approaches. The vibration forces in the track due to the passage of a train are by nature three-dimensional and a complete analysis undoubtedly requires a model of three-dimensional wave propagation. The aim of this paper is to investigate the quality of the information that can be gained from a two-dimensional model of a railway tunnel. The vibration transmission from the tunnel floor to the ground surface is analysed for the frequency range relevant to the perception of whole body vibration (about 4–80 Hz). A coupled finite element and boundary element scheme is applied in both two and three dimensions. Two tunnel designs are considered: a cut-and-cover tunnel for a double track and a single-track tunnel dug with the New Austrian tunnelling method (NATM).

1. Introduction

In recent years great interest has been shown in reduction of vibration in buildings caused by railway traffic. This is a concern both in the design of new railways and in the modification of existing ones. In densely populated areas, trains often run in tunnels. At these locations the transmitted vibration is an important environmental issue [1] and numerical models are required to complement empirical prediction models [2] and for tunnel structure design [3].

For each of these purposes, two-dimensional models have been used; even if the problem is by nature three-dimensional, see, for example, Ref. [4]. Justification for this is based on the fact that the train may be regarded

*Corresponding author. Tel.: +45 9635 8455; fax: +45 9814 2555.
E-mail address: la@civil.aau.dk (L. Andersen).

0022-460X/$ - see front matter © 2006 Elsevier Ltd. All rights reserved.
doi:10.1016/j.jsv.2005.08.044

as a long line of incoherent vibration sources. However, rather than using models to provide predictions of absolute vibration levels, they are more likely to be used to predict the effects of *changes* made to the tunnel structure [2,3], and it is assumed that such *changes* are reasonably predicted using a two-dimensional model.

The main reason that a two-dimensional model is preferred is that the numerical analysis with a three-dimensional model requires far more computing time such that it precludes parametric study. This remains the case even though, recently, so-called 'two-and-a-half-dimensional models', which calculate a three-dimensional field from a two-dimensional geometry, have been developed [5,6].

Here, two tunnel structures are considered. Firstly, a cut-and-cover tunnel with masonry abutment walls is analysed with both a two- and a three-dimensional model. The performance of the two-dimensional model is tested against that of the three-dimensional model in the comparison of different designs of the tunnel floor. Secondly, a tunnel is analysed, which has been built using the New Austrian tunnelling method (NATM) [7]. The changes in the response to either a change in the tunnel depth or the application of a wave impeding block (WIB) under the tunnel floor are compared with both a two- and a three-dimensional model.

The models are based on the combined finite element (FE) and boundary element (BE) methods. Solid FEs or BEs are used to model the tunnel. BEs are used to model the surrounding soil. Here the BE method is superior to the FE method due to its inherent ability to model radiating waves. Computer programs for both two- and three-dimensional elastodynamic coupled structure–soil analysis in the frequency domain have been developed. A detailed description of the FE method for elastodynamic analysis may be found, for example, in the book by Petyt [8]. The BE part of the model is an extension of the theory presented by Domínguez [9], which has been modified to account for open domains and to allow coupling with FEs. Here standard three-noded elements are used in the two-dimensional analysis and nine-noded quadrilateral elements are applied in the three-dimensional analysis.

2. Theory

2.1. Boundary elements for an open domain

In the frequency domain, the equation of motion and the boundary conditions for a viscoelastic two- or three-dimensional body Ω with the surface Γ read

$$\frac{\partial \sigma_{ij}(\mathbf{x},\omega)}{\partial x_j} + \rho B_i(\mathbf{x},\omega) + \omega^2 \rho U_i(\mathbf{x},\omega), \tag{1}$$

$$\left.\begin{array}{ll} U_i(\mathbf{x},\omega) = \hat{U}_i(\mathbf{x},\omega) & \text{for } \mathbf{x} \in \Gamma_U \\ P_i(\mathbf{x},\omega) = \hat{P}_i(\mathbf{x},\omega) & \text{for } \mathbf{x} \in \Gamma_P \end{array}\right\}, \quad \Gamma = \Gamma_U \cup \Gamma_P, \quad \Gamma_U \cap \Gamma_P = \emptyset. \tag{2}$$

Here $U_i(\mathbf{x},\omega)$ is the complex amplitude of the displacement field, $\rho B_i(\mathbf{x},\omega)$ are the body forces and $\sigma_{ij}(\mathbf{x},\omega)$ are the stresses that may be computed from the displacements by the constitutive relation. As indicated in Eq. (2) the displacement amplitude $U_i(\mathbf{x},\omega)$ is given on one part of the boundary, Γ_U, and the surface traction $P_i(\mathbf{x},\omega) = \sigma_{ij}(\mathbf{x},\omega)n_j(\mathbf{x})$ is given on the remaining part of the boundary, Γ_P. Here $n_j(\mathbf{x})$ are the components of the outward unit normal to the surface. In two dimensions the indices are 1, 2, and in three dimensions the indices are 1, 2, 3. Summation is performed over repeated indices.

In order to obtain the BE formulation of Eq. (1), a second state $U^*_{il}(\mathbf{x},\omega;\mathbf{y})$ is identified as the solution to the equation of motion

$$\frac{\partial \sigma^*_{ijl}(\mathbf{x},\omega;\mathbf{y})}{\partial x_j} + \rho\delta(\mathbf{x}-\mathbf{y})\delta_{il} + \omega^2 \rho U^*_{il}(\mathbf{x},\omega;\mathbf{y}), \tag{3}$$

where $\delta(\mathbf{x}-\mathbf{y})$ is the Dirac delta function and δ_{il} is the Kronecker delta. $U^*_{il}(\mathbf{x},\omega;\mathbf{y})$ is coined the fundamental solution, or the Green's function, and provides the response at the receiver point $\mathbf{x}$ in coordinate direction i to a concentrated point force applied at the source point $\mathbf{y}$ in direction l, with the circular frequency ω and unit amplitude. The fundamental solution is based on wave propagation in the full space and therefore only represents body waves emanating from the source, i.e. dilatation and shear waves with phase velocities c_P and

c_S, respectively. In three dimensions, $U^*_{il}(\mathbf{x},\omega;\mathbf{y})$ has a singularity of the order $1/r$, whereas the geometric dissipation in two dimensions is only of the order $1/\sqrt{r}$. This difference should be kept in mind when two- and three-dimensional models of wave propagation are compared.

The fundamental solution is applied as a weight function in the weak formulation of the equation of motion (1) for the physical field and vice versa. After some manipulations, and disregarding body forces in the interior of the domain Ω, Somigliana's identity is derived:

$$C_{il}(\mathbf{x})U_i(\mathbf{x},\omega)+\int_\Gamma P^*_{il}(\mathbf{x},\omega;\mathbf{y})U_l(\mathbf{y},\omega)\,\mathrm{d}\Gamma=\int_\Gamma U^*_{il}(\mathbf{x},\omega;\mathbf{y})P_l(\mathbf{y},\omega)\,\mathrm{d}\Gamma. \tag{4}$$

Here $P^*_{il}(\mathbf{x},\omega;\mathbf{y})$ is the surface traction related to the Green's function, $U^*_{il}(\mathbf{x},\omega;\mathbf{y})$. A full description and derivation of Eq. (4) may be found in Ref. [9]. $C_{il}(\mathbf{x})$ only depends on the geometry of the surface Γ at the observation point. On a smooth part of the surface $C_{il}(\mathbf{x})=1/2\delta_{il}$. For other geometries, e.g. a corner, $C_{il}(\mathbf{x})$ takes other values. A general procedure, which may be used for the evaluation of the geometry constants, is discussed below.

To obtain the BE formulation, the state variable fields on the boundary are discretized. Let $\mathbf{P}_j(\omega)$ and $\mathbf{U}_j(\omega)$ be the vectors storing the displacements and tractions at the N_j nodes in element j. The displacement and traction fields over the element surface Γ_j then become

$$\mathbf{U}(\mathbf{x},\omega)=\mathbf{\Phi}_j(\mathbf{x})\mathbf{U}_j(\omega),\quad \mathbf{P}(\mathbf{x},\omega)=\mathbf{\Phi}_j(\mathbf{x})\mathbf{P}_j(\omega), \tag{5}$$

where $\mathbf{\Phi}_j(\mathbf{x})$ is a matrix storing the interpolation, or shape, functions for the element. This allows the unknown values of the state variables to be taken outside the integrals in Eq. (4).

Finally, the two- or three-row matrices originating from Eq. (4) for each of the observation points may be assembled into a single matrix equation for the entire BE domain,

$$\mathbf{HU}=\mathbf{GP}. \tag{6}$$

Component (i,k) of the matrices $\mathbf{H}$ and $\mathbf{G}$ stores the influence from degree-of-freedom k to degree-of-freedom i for the traction and the displacement, respectively, i.e. the integral terms on the left- and right-hand side of Eq. (4). The $C_{il}(\mathbf{x})$ terms are absorbed into the diagonal of $\mathbf{H}$. In the present analysis, the coupling of the BE and FE models is carried out in terms of nodal forces (see Section 2.2), i.e. contributions from the surface traction on different elements adjacent to a node are transferred to nodal forces via the shape functions. $\mathbf{G}$ is thus a square matrix whereas in the native BE formulation $\mathbf{G}$ stores the influence from each element adjacent to a collocation node separately in order to provide a means of representing discontinuous surface traction over element edges.

Generally, the integrals of the $\mathbf{H}$ and $\mathbf{G}$ matrices are calculated using Gauss–Legendre quadrature. However, at the forcing point the Green's function for the surface traction is strongly singular of the order $1/r$ in two dimensions and $1/r^2$ in three. The diagonal terms of $\mathbf{H}$ thus have to be treated with caution. As proposed by Domínguez [9], the traction Green's function matrix is decomposed into its static part $\mathbf{H}^S$ and the dynamic (frequency dependent) residual part $\mathbf{H}^R$. By rigid-body-motion considerations, the diagonal terms of $\mathbf{H}$ for a closed interior BE domain may then be calculated as

$$\mathbf{H}_{ii}=\mathbf{H}^S_{ii}+\mathbf{H}^R_{ii}=\mathbf{H}^R_{ii}-\sum_{k=1,k\neq i}^{N}\mathbf{H}^S_{ik}, \tag{7}$$

where N is the total number of degrees of freedom in the BE discretization. Note that the geometry constants are absorbed in $\mathbf{H}^S$. Hence they are determined simultaneously with the singular terms of the traction Green's function matrix. This is an advantage over nonlinear coordinate transformation techniques [11], in which the geometry constants must be determined separately.

Unfortunately, the rigid-body-motion technique will only work for a closed domain. For an open domain, such as the soil in the present case, Ahmad and Banerjee [12] proposed the use of so-called *enclosing elements*, where a number of elements are added to transform the open domain into a closed domain, entirely for the evaluation of the $\mathbf{H}^S$ diagonal terms. The $\mathbf{H}^S$ terms need only be calculated once and can then be used at all frequencies of the analysis.

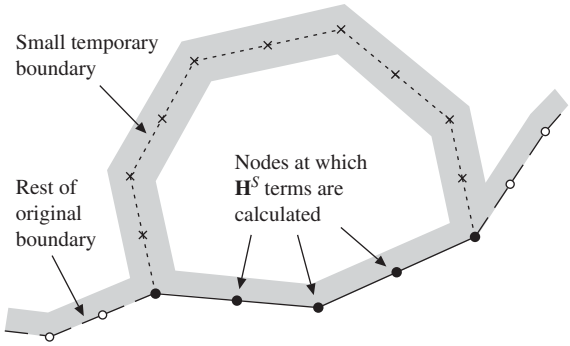

Fig. 1. 'False' local boundary for the evaluation of diagonal terms in the static part of the traction Green's function matrix.

Instead of creating a closed domain for the entire domain at once, Jones et al. [13] suggested that a 'false' local boundary is formed for a few nodes at a time (see Fig. 1). They gave a detailed description for the two-dimensional case, whereas Andersen and Jones [14] treated the three-dimensional case. The idea is that the geometrical constants $C_{ik}(\mathbf{x})$ only depend on the local geometry, and the singularities of the traction Green's function arise in the contributions from a node to itself. Hence only the local geometry of the surface need be modelled correctly. The advantages of this method over the fully enclosing-elements technique are that the local boundaries are more easily generated in an automatic manner, and that the technique may be applied to any domain, open or closed. It is also faster to solve multiple small systems of equations for the local false surfaces than to solve one big system of equations for a single global enclosure.

2.2. Coupling of FE and BE schemes

For some parts of the structure, the use of a BE region is not appropriate, either because the material is not homogeneous over a large part of the structure or because the structure is thin. In these parts of the model FEs may be used. In the present analyses, isoparametric FEs with quadratic interpolation functions are applied. However, in parts of the concrete structure that are much stiffer than the surrounding soil and masonry (i.e. wavelengths are much longer) linear interpolation is used across the thickness in the three-dimensional model so that the number of degrees of freedom is kept to a minimum.

In order to couple a BE domain formulated in terms of surface tractions with an FE region with loads applied in terms of nodal forces, a transformation matrix $\mathbf{T}$ is defined, such that $\mathbf{F} = \mathbf{TP}$. Here $\mathbf{F}$ is the vector of nodal forces equivalent to the tractions $\mathbf{P}$ applied on the domain. The transformation matrix only depends on the spatial interpolation functions, i.e. the shape functions, for the elements along the interaction boundary. Hence, $\mathbf{T}$ may be determined once and for all and applied in all analyses with a given model geometry. Subsequently, for each frequency the matrix

$$\mathbf{TG}^{-1}\mathbf{H} = \mathbf{K}_{\mathrm{BE}} \tag{8}$$

defines an *equivalent dynamic stiffness matrix* for the BE domain. The coupled model is illustrated in Fig. 2, and as indicated operation (8) turns the BE domain into a macro FE. In contrast to the dynamic stiffness matrix, which is obtained in the FE method (see below), $\mathbf{K}_{\mathrm{BE}}$ is fully populated and asymmetrical.

In the frequency domain, the equation of motion for an FE region takes the well-known form [8]

$$(-\mathbf{M}\omega^2 + \mathrm{i}\mathbf{C} + \mathbf{K})\mathbf{U} = \mathbf{K}_{\mathrm{FE}}\mathbf{U} = \mathbf{F}, \tag{9}$$

where $\mathbf{M}$ is the mass matrix and $\mathbf{K}$ is the static stiffness matrix. $\mathbf{C}$ is constructed from material loss factors and the element stiffness matrices in line with the hysteretic damping model used in the BE equations. For a single frequency of excitation the system matrices may be reduced to the dynamic stiffness matrix $\mathbf{K}_{\mathrm{FE}}$. Then the matrices $\mathbf{K}_{\mathrm{FE}}$ and $\mathbf{K}_{\mathrm{BE}}$ for a number of sub-domains may be assembled into a global dynamic stiffness matrix for the entire model. This may then be solved for the complex amplitude of displacement response to a set of forces applied to any of the nodes in the model.

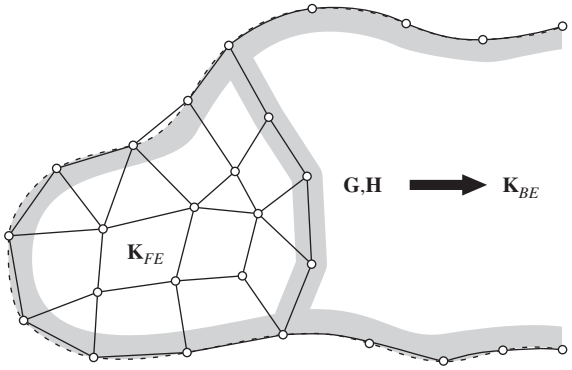

Fig. 2. Combined finite element and boundary element model. Loads are applied as nodal forces.

As an alternative to the coupling method described above, in which the global solution is carried out in a FE sense, the interaction forces between the FE part of the model and the BE domains may be described in terms of surface traction. This requires the implementation of a number of auxiliary equations in order to manage discontinuous traction around corners, etc. [10]. The coupling in terms of nodal forces has been selected in the present work due to its simplicity.

3. Analysis of a cut-and-cover tunnel

Three cut-and-cover tunnel structures are analysed. In Section 3.1 the structures are described, and in Section 3.2 the results of a two- and a three-dimensional model are compared.

3.1. Tunnel structure models

The first tunnel (referred to as Model 1 and shown in Fig. 3) represents the basis for comparison against which structural changes have been made. It is 7.0 m deep, 12.0 m wide and accommodates two railway tracks. The abutment walls have a thickness of 2.0 m and consist of masonry. The roof is 1.0 m deep and is attributed properties to achieve a realistic bending stiffness and mass for a bridge roof that would usually be a composite steel beam and concrete construction.

There is no floor; the tracks rest directly on the ground. The tracks are not modelled; a unit load representing that exerted by the track is applied on the tunnel floor at the right-hand track position (Fig. 3). The entire structure is surrounded by a homogeneous half-space of drained sandy soil.

In each of the Models 2 and 3 changes are applied to the tunnel structure.

- *Model 2*: The soil underneath the abutment walls is stiffened to a depth of 13 m.
- *Model 3*: The soil at the tunnel floor is replaced with a 1 m deep concrete slab.

Material properties for each of the model components are listed in Table 1, and Fig. 3 shows the combined two-dimensional FE/BE mesh. The BEs are all 2 m long, and the FEs have the dimensions $2 \times 1\,\mathrm{m}^2$. This ensures a minimum of approximately three quadratic elements per wavelength at 80 Hz, which has been found to be satisfactory [14]. In the two-dimensional model, a vertical load is applied over a 2 m wide strip with a total intensity of 1 N/m (in the along-tunnel direction). The three-dimensional model is constructed as an extrusion of the model in Fig. 3 and the 1 N load is applied over an area of $2 \times 2\,\mathrm{m}^2$, i.e. a single quadrilateral BE.

The three-dimensional mesh is 22 m long in the track direction; 10 m on either side of the load. Use has been made of the lateral symmetry of the structure for efficiency. The analysis is carried out twice. In the first case the load is applied symmetrically, and in the second case it is applied anti-symmetrically around the plane of

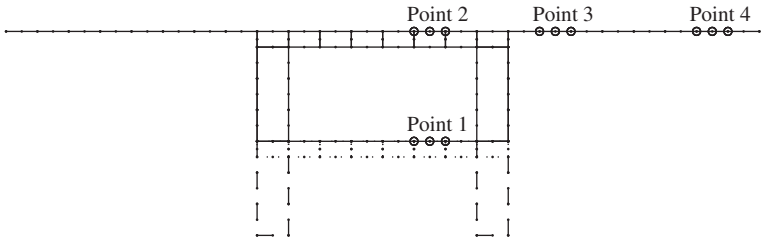

Fig. 3. Layout of the two-dimensional cut-and-cover tunnel models. Point forces are applied at the nodes indicated as 'Point 1'. The fully drawn part corresponds to Model 1, i.e. the reference model. Dashed parts (– –) are introduced in Model 2, and dotted parts (· · · · ·) are introduced in Model 3.

Table 1
Material properties

Material	E (MPa)	v	ρ (kg/m^3)	η
Concrete	20,000	0.30	2400	0.03
Masonry	10,000	0.15	2400	0.50
Soil	1000	0.20	2000	0.10
Stiffened soil	5000	0.20	2100	0.10

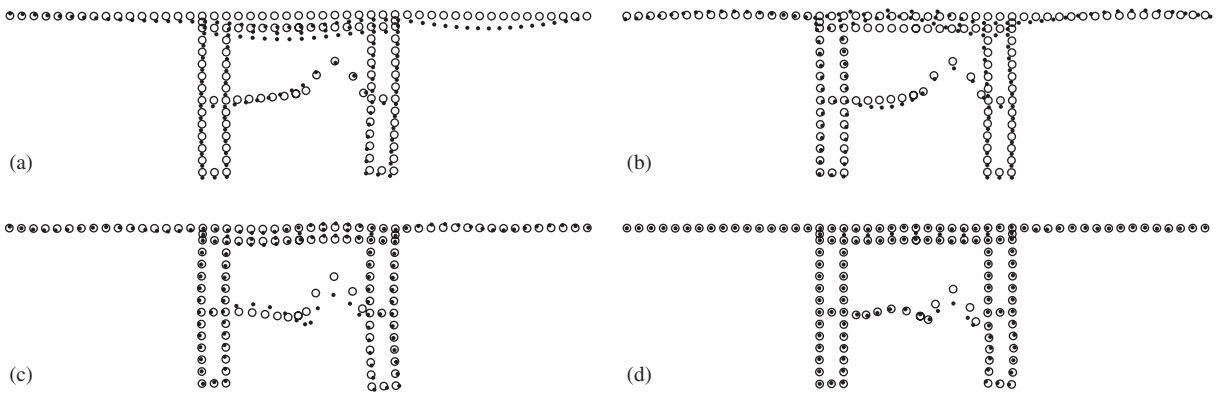

Fig. 4. Nodal displacements in Model 2 at the four frequencies: (a) 10 Hz; (b) 20 Hz; (c) 40 Hz; and (d) 80 Hz: • two-dimensional results, and ○ three-dimensional results.

symmetry. Subsequently the results are combined to obtain the response to an area load applied only to one of the tracks and with a total magnitude of 1 N.

In the two-dimensional case, the geometric dissipation (i.e. with distance due to spreading of the wave front) is smaller than in the three-dimensional case. In particular, Rayleigh waves are only subject to material damping. Consequently, the error where the computation model is truncated is greater in the two-dimensional model than in the three-dimensional case. However, a convergence study of the response in the two-dimensional model indicates that the errors due to truncation of the mesh are localized to a small area near the artificial edge, typically with an extent of one or two BEs. This is due to the fact that the impedance mismatch between the modelled half-space and the full space forming the basis of the Green's functions is small. Further, the ground surface far from the tunnel serves almost entirely as a receiver, i.e. there is only little back-coupling to the structure, see Fig. 4. Hence, the ground surface only needs to be taken to a distance of 24 m from the centre-line of the tunnel in both the two- and the three-dimensional case.

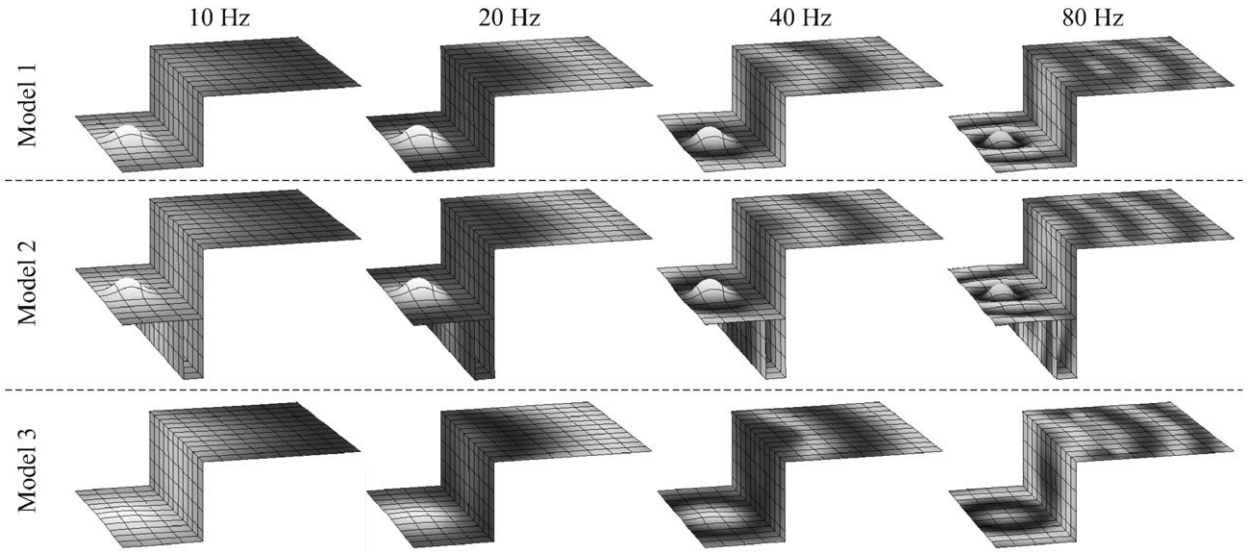

Fig. 5. Harmonic response of the three-dimensional BE/FE model of a cut-and-cover tunnel. The displacements are scaled by the factor 3×10^9. Dark and light shades of grey indicate negative and positive vertical displacements, respectively.

The response is calculated at the one-third octave band center frequencies from 4 to 80 Hz. Fig. 4 shows the superimposed response of the two- and three-dimensional models for results at 10, 20, 40 and 80 Hz in Model 2. The three-dimensional results have been scaled by a factor of three greater than the two-dimensional results in order to obtain a similar displacement at the load. The figure clearly shows that the geometric damping is much stronger in the three-dimensional case than in the two-dimensional one. Thus, at the surface of the half-space and the tunnel floor, the response in the three-dimensional model is about one to two orders of magnitude smaller than the response in the two-dimensional case despite the adjustment to make them similar near to the load.

To give an impression of the nature of the three-dimensional wave propagation, the response in the BE part of the model is illustrated in Fig. 5 for Models 1–3 at the frequencies 10, 20, 40 and 80 Hz. Note that only the BE domains used to model the half-space and the foundation stiffening under the walls (Model 2) are shown. Further, in Model 3 the surface of the ground inside the tunnel lies 1 m below the level in the other two models due to the presence of the concrete floor, which has been modelled with FEs.

3.2. Response differences due to the design changes

Next, the responses from the three different tunnel structures are compared. In particular the changes in the response due to the modifications applied to the structure in Models 2 and 3 are analysed. Following the findings of Ref. [2], that comparisons should be made on the basis of a combination of lateral and vertical calculated responses, the pseudo-resultant, R, is used,

$$R = \sqrt{|U_1|^2 + |U_2|^2}. \tag{10}$$

The symmetry of the models means that the out-of-plane lateral displacement amplitude U_3 in the three-dimensional model is equal to zero on the plane where the results are compared.

For the three-dimensional results, the rms value of the pseudo-resultants along a line parallel to the tunnel has been used. This corresponds to the response measured at a single location from a series of passing incoherent sources as a train passes. The results along a line on the surface of the ground and perpendicular to the tunnel axis are compared with the pseudo-resultants computed with the two-dimensional model.

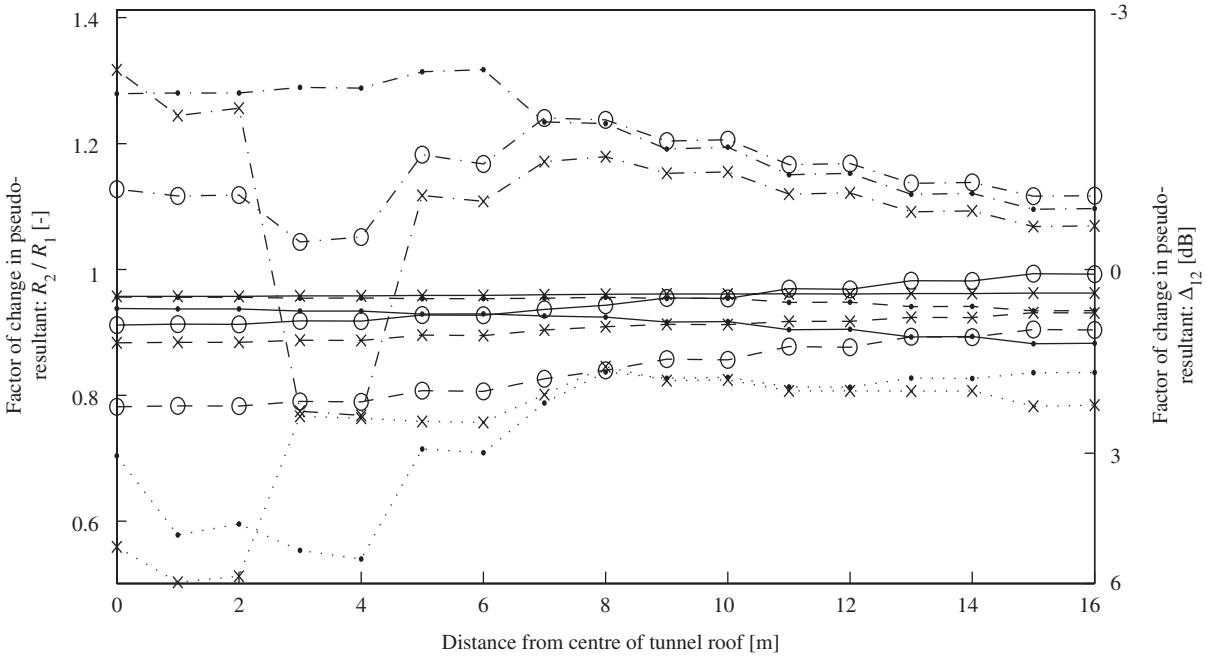

Fig. 6. Factor of change in pseudo-resultant response between cut-and-cover tunnel Models 1 and 2 for three-dimensional models. Δ_{12} is defined by Eq. (11). The results are compared along a line on the ground surface perpendicular to the tunnel axis. The rms value of the response to nine loads applied along the tunnel has been taken. Lines indicate different frequencies, — (5 Hz), – – (10 Hz), – · (20 Hz), · · · (40 Hz); points indicate different tunnel model lengths, • ($L = 26$ m), × ($L = 50$ m), and ○ ($L = 98$ m).

A convergence study of the pseudo-resultant response in the two- and three-dimensional models has been carried out in order to investigate whether the differences in the response obtained with the two models are due to errors introduced into the models by their truncation at finite lengths either in:

- the distance from the tunnel to the truncation edge parallel with the tunnel axis (both in the two- and the three-dimensional tunnel models),
- the length of the modelled tunnel section (only in the three-dimensional model).

As mentioned previously, the impedance mismatch between the modelled half-space and the full space adopted in the Green's functions is small. Therefore, convergence is reached with only few elements between the tunnel and the truncation edge in both the two- and the three-dimensional models. However, in the three-dimensional model the convergence rate is poor with respect to the length of the modelled tunnel section, see Fig. 6. In particular the response of the tunnel roof converges slowly as the tunnel model length is increased. This is due to the strong impedance mismatch between the thin tunnel roof (a plate) and the full space. The inclusion of small BE domains at the artificial ends of the tunnel roof almost corresponds to the prescription of Dirichlet conditions $U_i(\mathbf{x}, \omega) = 0$ at the artificial ends of the tunnel roof. This only provides a small improvement compared with a model in which the continuous tunnel roof is modelled as a plate with finite length, i.e. Neumann conditions of the kind $P_i(\mathbf{x}, \omega) = 0$ are given on the truncation edge.

In order to provide a better model of the tunnel roof with infinite length along the tunnel, transmitting boundary conditions based on the Green's function for a plate could be employed. However, in the present study use has been made of the small BE domain termination. The response on the roof in the three-dimensional model should be treated with caution, but as indicated by Fig. 6 there is a good convergence of the response along the surface of the ground outside the tunnel.

Fig. 7 shows the results of the two- and three-dimensional cut-and-cover models at the frequencies 10, 20, 40 and 80 Hz. As would be expected, there is a general attenuation of the vibration with distance from the centre of the tunnel in both the two- and the three-dimensional models. For the frequencies 10, 20 and 40 Hz, the

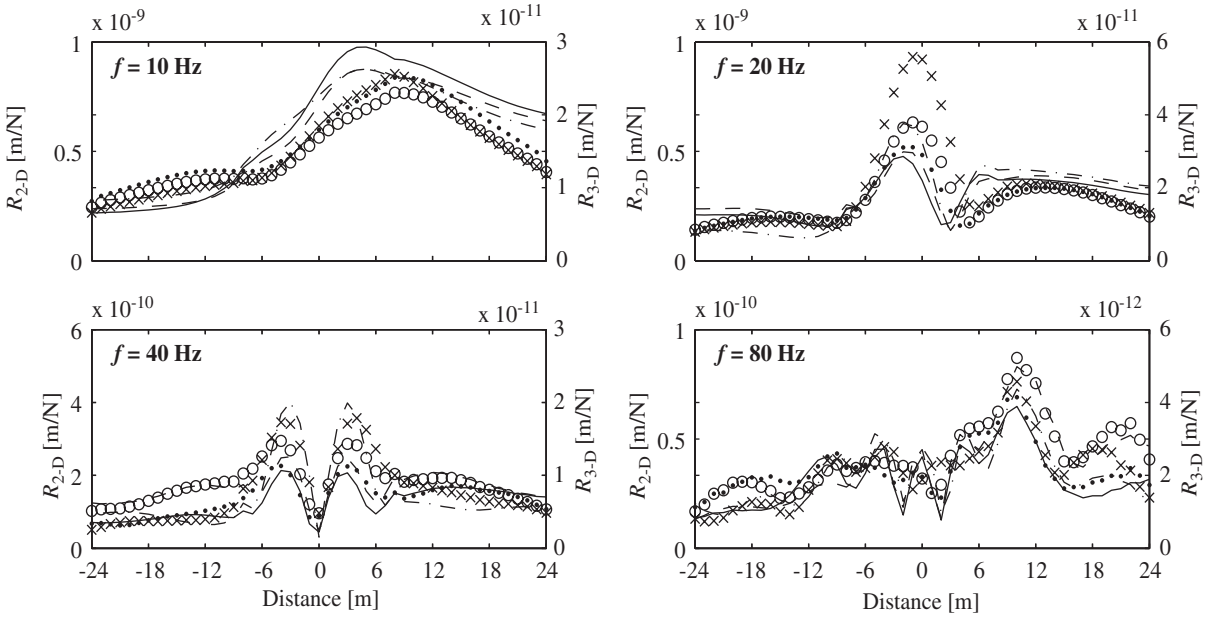

Fig. 7. Pseudo-resultant response along the surface of the ground versus distance from the centre of the tunnel. The roof ranges from −6 to 6 m. Lines indicate two-dimensional results, — (Model 1), – – (Model 2), – · (Model 3); points indicate three-dimensional results, • (Model 1), ○ (Model 2), and × (Model 3).

maximum response is located somewhere on the roof (−6 to 6 m). However, at 80 Hz there is a strong local amplification in the soil just outside the tunnel. The two- and three-dimensional models predict similar behaviour particularly at the higher frequencies. This was to be expected since material damping dominates over geometrical damping at high frequencies. However, Fig. 7 does not show clearly whether the *changes* are predicted similarly.

In order to quantify changes in the response, Δ_{12} and Δ_{13} (expressed in dB) are introduced as the factors of change of the pseudo-resultant between Models 1, and 2 or 3,

$$\Delta_{1k} = 20\log_{10}\left(\frac{R_1}{R_0}\right) - 20\log_{10}\left(\frac{R_k}{R_0}\right), \quad k = 2, 3. \tag{11}$$

Here R_1 is the pseudo-resultant response in Model 1 at a given point and R_k is the response in Model 2 or 3. Finally, $R_0 = 10^{-6}$ m is a reference value of the pseudo-resultant. As in Fig. 7, the rms response along a line parallel to the tunnel has been calculated from the three-dimensional model. Eq. (11) defines a positive Δ_{12} or Δ_{13} as a reduction in vibration in Model 2 or 3 compared with Model 1.

Δ_{12} and Δ_{13}, are calculated for the four 'points' shown in Fig. 3. Fig. 7 indicates that the pseudo-resultant response may change rapidly with distance, particularly at high frequencies so, to get a more stable measure of the response, the pseudo-resultant has been averaged over three nodes around each location (Fig. 3). The results are plotted in Fig. 8. They must be interpreted in the light of the findings from the convergence study. The results of the two-dimensional models are fully converged, i.e. within ± 0.1 dB, for all observation 'points'. As mentioned previously this is due to the small impedance mismatch between the modelled half-plane and the full space adopted in the Green's functions. The results of Fig. 6 suggest that the results of the three-dimensional model can be regarded converged to within ± 1 dB at Points 3 and 4 on the surface of the ground outside the tunnel, see Fig. 3. On the tunnel floor, close to the loading, the results are less affected by the edges of the model and, although not shown in Fig. 6, have been found to be constant to within ± 0.5 dB. However, on the roof, for the reasons discussed above, the results can only be regarded as having converged to within ± 3 dB. Thus, at Point 2 the errors due to mesh truncation are comparable to the changes in response to

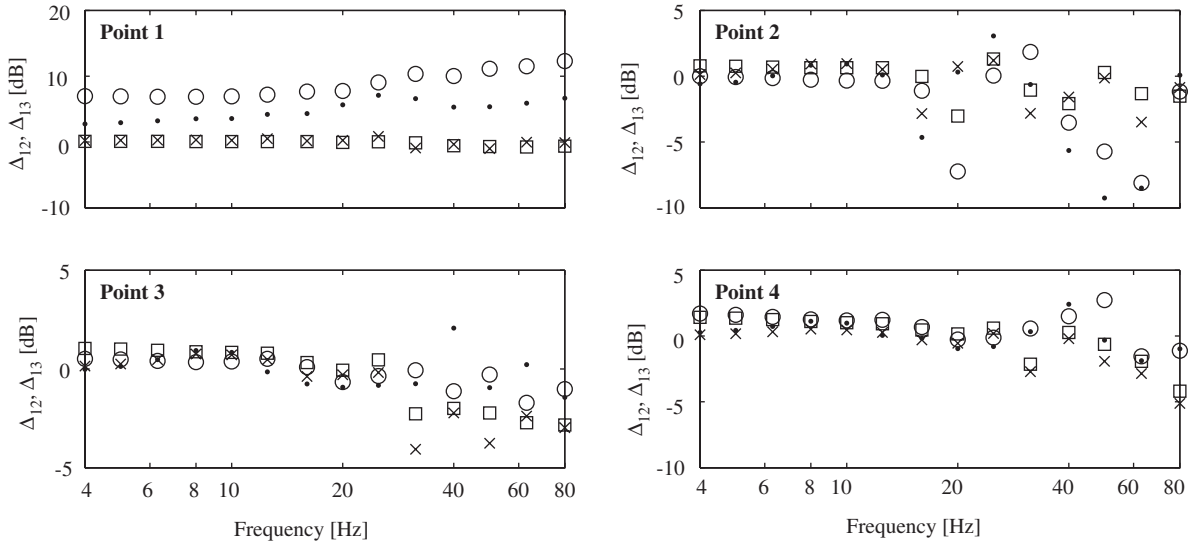

Fig. 8. Level difference spectra in the pseudo-resultants of the cut-and-cover tunnel models: □ (Δ_{12}−3-D), × (Δ_{12}−2-D), ○ (Δ_{13}−3-D) and • (Δ_{13}−2-D).

changes in the tunnel structure. Hence, only vague conclusions may be drawn from a comparison with the results of the two-dimensional model in this case.

Almost no change in the response is achieved at 10 Hz and lower frequencies. This observation can be made in both the two- and three-dimensional models. Only for Point 1, i.e. directly under the load, is there a consistent, significant change in the response, and only for Model 3. This decrease in response is due to the installation of the concrete floor. A reduction of 7–8 dB in the response is predicted in the three-dimensional analysis, whereas the reduction in the two-dimensional case is only about 3–4 dB.

At the surface of the ground 'far' from the tunnel (Point 4) the three-dimensional model indicates a small improvement in the low-frequency range. Installation of the concrete floor (Model 3) is slightly better than stiffening under the abutment walls (Model 2), though the changes are all below 3 dB. This however can be regarded as a significant difference at these locations given the uncertainties identified in Fig. 6. However, at Point 3, close to the tunnel, the soil stiffening is advantageous, whereas the concrete floor leads to a greater proportion of the energy from the source propagating up through the walls and into the soil nearby. The same trends are observed in the two-dimensional model, though the changes in the pseudo-resultant responses are less pronounced than in the three-dimensional case.

At higher frequencies, the agreement between the two models is poorer. At most frequencies there is a weak correspondence for Δ_{13}; but around 40–60 Hz both models predict a very perceptible vibration level increase of 6 dB on the roof. The results for Δ_{12} generally lie closer together. The concrete floor changes the propagation in the structure and soil much more than the soil stiffening does. Neither of the structural changes actually provides an improvement; the soil stiffening, indeed, turns out to be generally disadvantageous at frequencies above 20 Hz.

4. Analysis of a NATM tunnel

Now, a similar study is carried out for a NATM tunnel. The popularity of this method has increased over the last decades for deep tunnels in soil with medium stiffness, because the construction process is cheaper than boring as no specialized equipment is necessary. NATM tunnels are dug with the use of standard excavators, and the concrete lining is cast in situ [7].

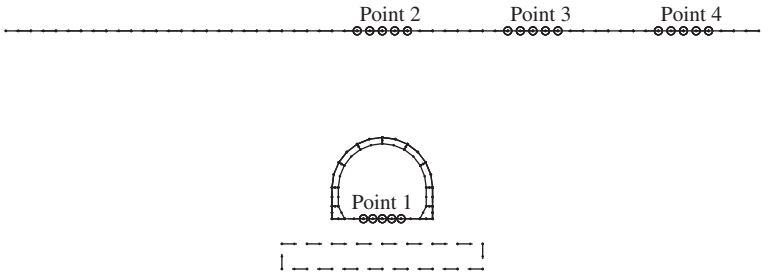

Fig. 9. Layout of the two-dimensional NATM tunnel models. Point forces are applied at the nodes indicated as 'Point 1'. The fully drawn part represents Model 1, i.e. the reference model. Dashed parts (– –) are introduced in Model 2, and Model 3 is identical to Model 1 except for the tunnel depth which is increased from 15 to 20 m.

4.1. Tunnel structure models

Two changes to a NATM tunnel are considered. For this purpose, three models are analysed, with Model 1 representing the basis for comparison, see Fig. 9.

- *Model 1*: The tunnel is 15 m deep, 7 m wide and accommodates a single track. The crown forms a circular arc with a maximum height of 6 m above the tunnel floor. The upper part of the walls and the crown are lined with concrete having a thickness of 0.5 m. The wall thickness is increased linearly inside the tunnel from 0.5 m, 1 m above the floor, to 1 m at the floor. The floor is 15 m below the ground surface.
- *Model 2*: A WIB of stiffened soil is situated 2 m below the tunnel floor. The block is 2 m deep and 16 m wide, thus extending 4 m on either side of the tunnel. Note that replacement of the original soil with concrete is unrealistic. Instead, a strengthening of the existing soil in situ by, for example, 'jet grouting' [15] is considered. WIBs have been proposed to reduce low-frequency vibration from a railway track. Amongst others, Takemiya et al. [16] analysed the effect of a WIB in a railway embankment, and Chouw and Pflanz [17] found that a WIB in a half-space reduces the far-field vibration from a moving vertical load applied over it.
- *Model 3*: The tunnel is deeper in the ground so that the floor is 20 m below the surface. This case tests the ability to predict the vibration at one tunnel from vibration measurements made at another existing site.

In the two-dimensional analysis, a harmonic vertical strip load of 1 N/m, 3 m wide, is applied on the centre of the tunnel floor. In the three-dimensional analysis, a load with a total magnitude of 1 N is applied over the rectangular area $3 \times 4\,\mathrm{m}^2$ corresponding to two BEs.

The material properties used in the models are listed in Table 1, and the element meshes of the two-dimensional models are illustrated in Fig. 9. In these, 15, 2 m long elements make up the ground surface on either side of the plane of symmetry. In the three-dimensional analysis, seven elements with the dimensions $4 \times 4\,\mathrm{m}^2$ are used. Numerical experiments show that nodes belonging to these elements work as receiver points only, thus having negligible influence on the response of the model. Hence, relatively few elements can be used in the three-dimensional surface model.

The three-dimensional wave propagation pattern in Models 1–3 is illustrated in Fig. 10 at 10, 20, 40 and 80 Hz. The vibration at the surface of the ground is changed dramatically by both structural changes, whereas only the WIB influences the response at the tunnel floor. Thus in Models 1 and 3, surface waves of the same character propagate along the floor of the tunnel. Near the walls, the wavelength in the soil is increased due to interaction with the stiffer structure.

4.2. Response differences due to the design changes

As for the cut-and-cover tunnel, a convergence study has been carried out in order to verify that the discrepancies between the responses in the two- and three-dimensional models are not due to mesh truncation. Since the nodes on the surface of the ground have little effect on the response, the truncation edge can be

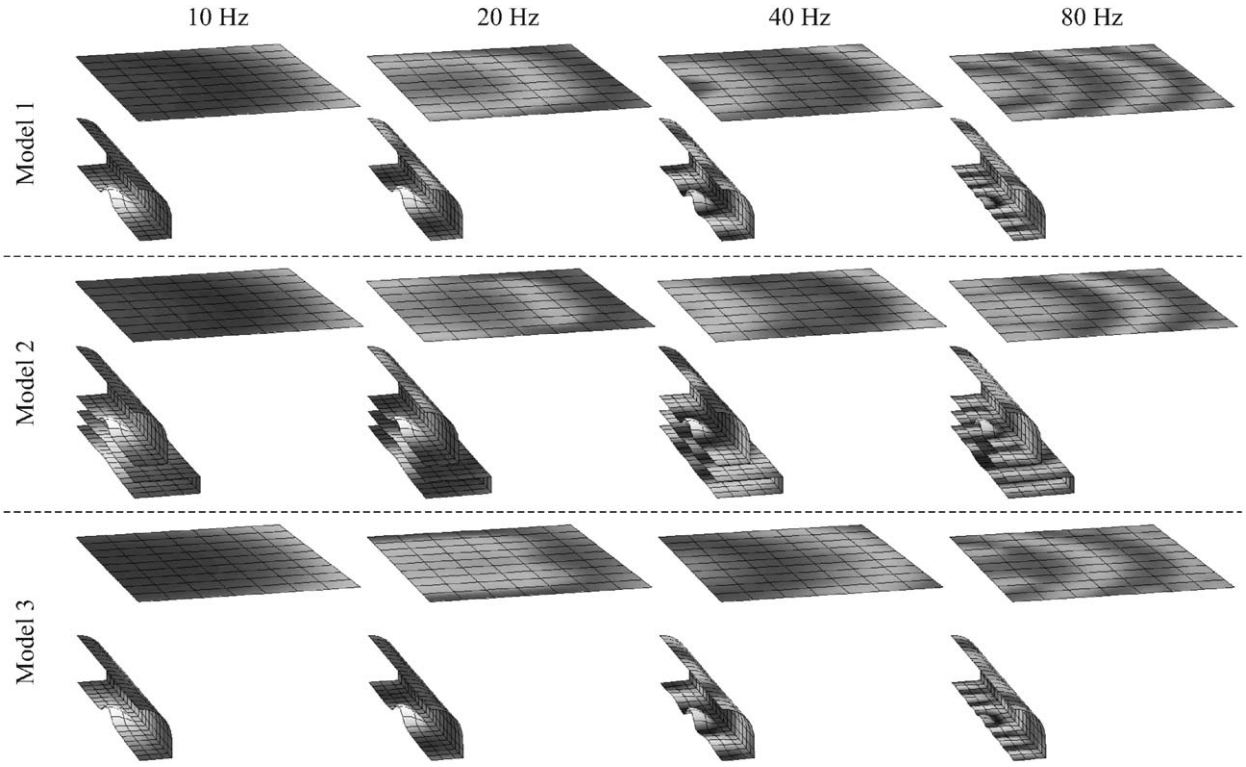

Fig. 10. Harmonic response of the three-dimensional BE/FE model of a NATM tunnel. The displacements are scaled by the factor 3×10^9. Dark and light shades indicate negative and positive vertical displacements, respectively.

placed close to the tunnel. Further, the rate of convergence with respect to the tunnel length is much better in the present case than for the cut-and-cover tunnel model as illustrated in Fig. 11, in which the rms pseudo-resultants in Models 1 and 3 are compared for the frequency 20 Hz. This stems from the fact that the impedance of the half-space with the embedded tunnel is close to that of a homogeneous half-space and therefore similar to that of the full space assumed in the Green's functions. As indicated in the figure, the results can be regarded converged to within ± 1 dB for Points 2, 3 and 4 on the surface of the ground, see Fig. 9. As in the case of the cut-and-cover tunnel, the convergence is better at Point 1 where the load is applied.

Fig. 12 shows the pseudo-resultant response along the ground surface for the NATM tunnel models at 10, 20, 40 and 80 Hz. As before, the rms value for sources along the track is computed for the three-dimensional model in order to simulate the effect of a passing train. The response is symmetric around the tunnel because the load is applied symmetrically.

Although a general qualitative agreement in the trends of response with distance between two- and three-dimensional models exists, differences between the results can clearly be seen. The worst case of disagreement in this respect is present at 20 Hz where the two-dimensional models show a maximum of vibration over the tunnel whereas the three-dimensional models all show a minimum there. Similar differences can be found in the 40 and 80 Hz graphs. The reason for the different behaviour in the two- and three-dimensional models is the fact that the load in the two-dimensional model is applied in phase at all points along the tunnel, whereas in the three-dimensional model the load is applied as a number of incoherent sources. This implies that negative interference between waves emanating from different points along the track does not take place in the three-dimensional model.

Using the same approach as for the cut-and-cover case, the level difference spectra Δ_{12} and Δ_{13} at the tunnel floor and three (averaged) points along the surface (Fig. 9) are presented in Fig. 13. At the tunnel floor (Point 1) the response is almost identical in Models 1 and 3, i.e. the distance to the ground surface has insignificant effect at the tunnel. The two- and three-dimensional models predict the same qualitative behaviour, but the

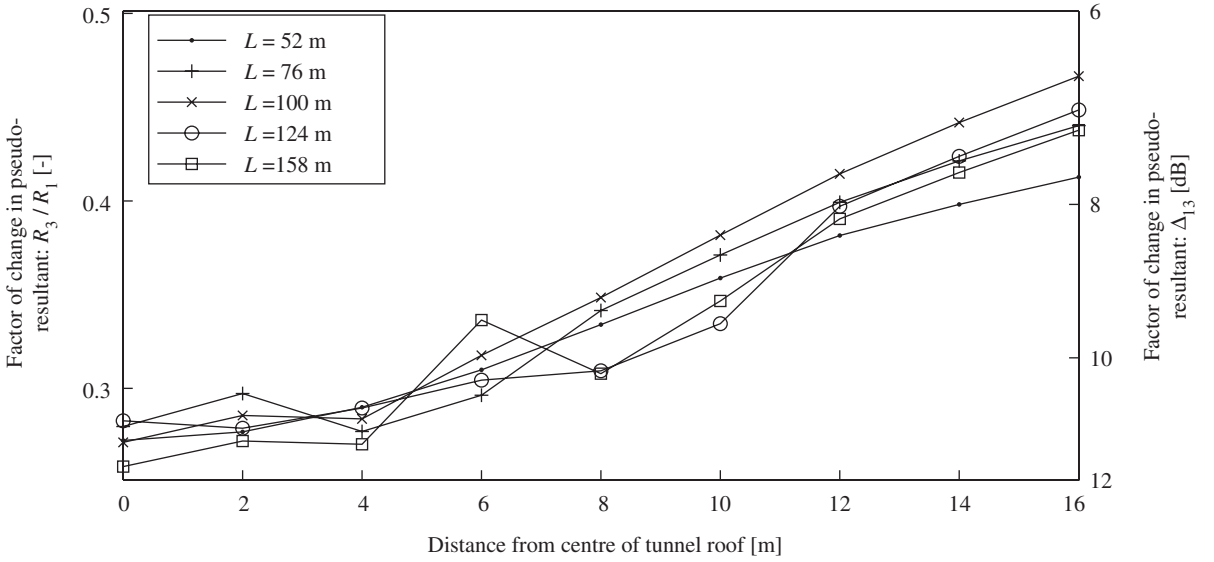

Fig. 11. Factor of change in pseudo-resultant response between NATM tunnel Models 1 and 3 for three-dimensional models with different lengths, L. Δ_{13} is defined by Eq. (11). The results are compared along a line on the ground surface perpendicular to the tunnel axis. The rms value of the response to nine loads applied along the tunnel for the frequency 20 Hz has been taken.

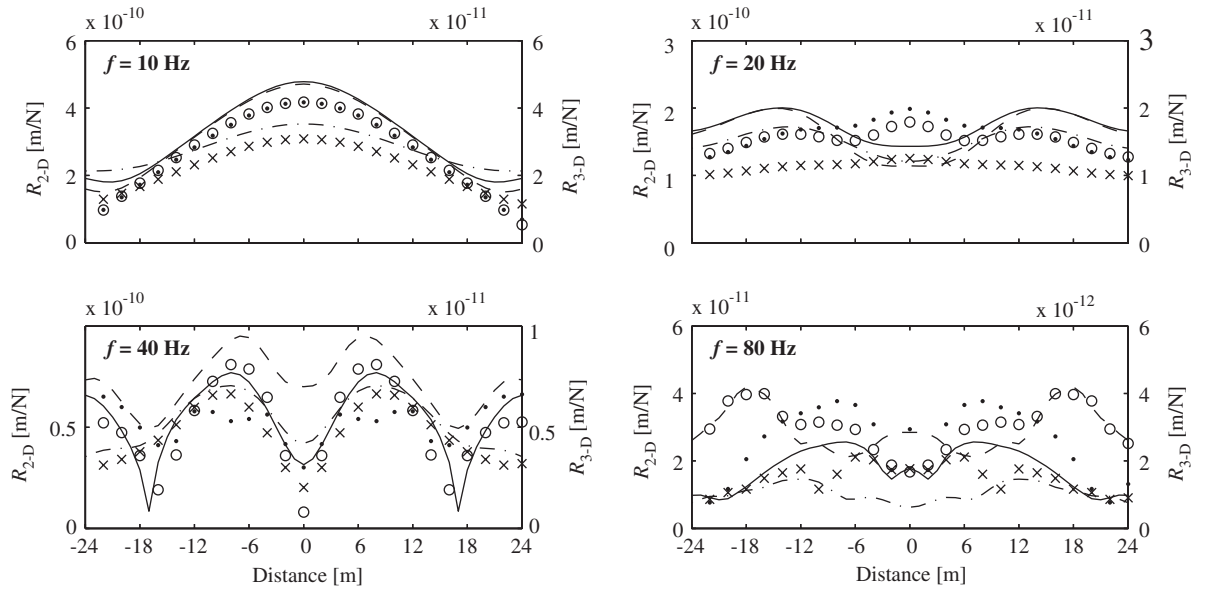

Fig. 12. Pseudo-resultant response along the surface of the ground over the NATM tunnel versus distance from the tunnel centre-line. Lines indicate two-dimensional results, — (Model 1), – – (Model 2), – · (Model 3); points indicate three-dimensional results, • (Model 1), ○ (Model 2), and × (Model 3).

change in response is predicted to be slightly greater in the latter case. The wave-impeding block leads to a decrease in the response under the load in the frequency range up to 60 Hz, but an increase at 80 Hz. Here both the two- and three-dimensional models predict resonance in the soil above the WIB. On the surface, however, the WIB has little effect, whereas the increase of tunnel depth results in greater changes.

In the case of both changes to the geometry, immediately above the tunnel (Point 2) the two- and three-dimensional models predict similar changes for frequencies below 31.5 Hz; but in most cases the change is very

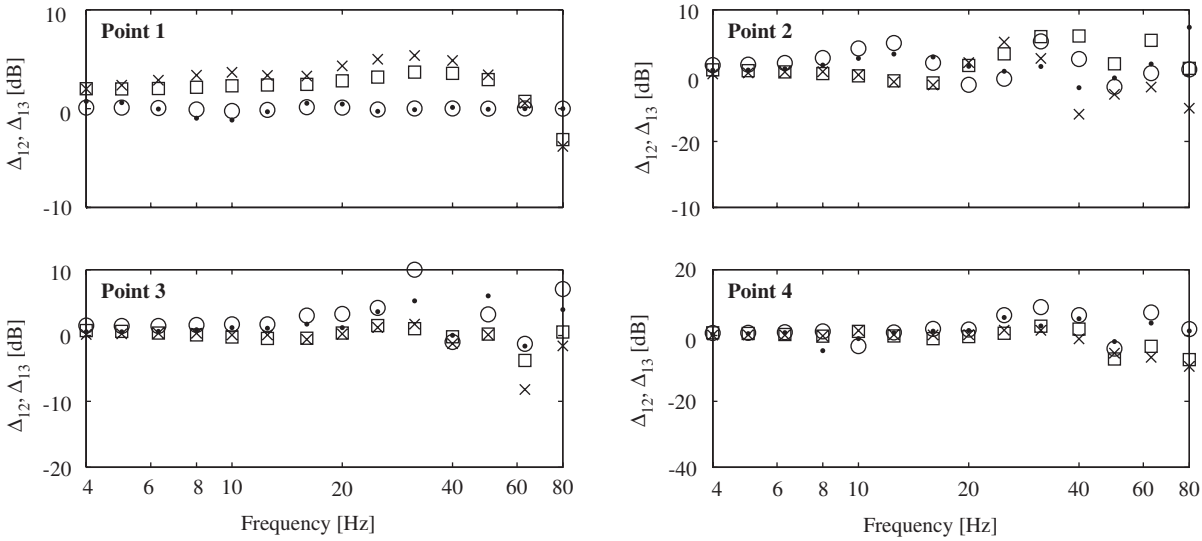

Fig. 13. Level difference spectra in the pseudo-resultants of the NATM tunnel models: □ (Δ_{12}−3-D), × (Δ_{12}−2-D), ○ (Δ_{13}−3-D) and • (Δ_{13}−2-D).

small. Although many of the points above this frequency can be said to agree, there are a number of instances where there is a significant difference at particular frequencies. Again, this is a result of the fact that the load in the two- and three-dimensional models is applied as a strip load and a number of incoherent sources, respectively.

5. Conclusions

Two- and three-dimensional combined finite and boundary element analyses have been carried out for two railway tunnel structures. The aim has been to investigate, what information can reliably be gained from a two-dimensional model to aid a tunnel design process or an environmental vibration prediction based on 'correcting' measured data from another tunnel in similar ground.

In the case of both types of tunnel examined, only small changes in the vibration response are predicted from the structural changes made. This also makes it difficult to calculate reliable changes in vibration level because of the necessary truncations of the model surfaces. This applies to the three-dimensional model in particular. The changes although of only a few dB are realistic and furthermore are significant in the perception of vibration. The studies therefore do represent a realistic situation for which the models could be used.

For both tunnels there is a similar trend in the wave pattern in the two- and three-dimensional models. Both the two- and the three-dimensional models show only small changes to the response at the surface of the ground, particularly at low frequencies. Qualitatively, a two-dimensional model is shown by these two examples to be useful to indicate whether reductions in the vibration can be achieved when the structure is changed. Apparently the two-dimensional model produces more useable results for this purpose when the structure is buried in the ground than when a structure near the surface is analysed. Further, the accuracy increases with the distance from the tunnel. In addition to this, a three-dimensional coupled BE and FE model of a cut-and-cover tunnel is not easily made. The main difficulty lies in a proper modelling of the continuous roof, and future models may be improved by the implementation of transmitting boundary conditions for a plate.

When deciding whether a two- or three-dimensional model should be used, the computational cost may be of importance. The analysis of the tunnel models in the present work takes about five seconds per frequency in the two-dimensional case, whereas the computation time for the three-dimensional models is about 2 h per frequency on a P4-2.8 GHz PC. Thus, a full three-dimensional analysis takes approximately 1000–2000 times

longer than the two-dimensional analysis. This difference is increased when larger numerical models are considered.

Combined with the observation that two-dimensional models provide results that qualitatively agree with those of three-dimensional models at most frequencies, two-dimensional models may be preferred. However, the models do show significant differences in the predicted responses. The conclusion based on the experience of the present analyses is that a full three-dimensional model is required for absolute vibration transmission predictions and is to be preferred in order to obtain more accurate estimates of the changes in response due to changes in tunnel structure or depth.

Acknowledgements

Lars Andersen would like to thank the Danish Technical Research Council for financial support via the research project: 'Damping Mechanisms in Dynamics of Structures and Materials'.

References

[1] C.J.C. Jones, Using numerical models to find antivibration measures for railways, *Proceedings of the Institution of Civil Engineers, Transport* 105 (1994) 43–51.
[2] C.J.C. Jones, D.J. Thompson, M. Petyt, A model for ground vibration from railway tunnels, *Proceedings of the Institution of Civil Engineers, Transport* 153 (2002) 121–129.
[3] C.J.C. Jones, Groundborne noise from new railway tunnels, in: *Proceedings of Internoise 96*, Liverpool, UK, July/August, 1996, pp. 421–426.
[4] K.H. Chua, T. Balendra, K.W. Lo, Groundborne vibrations due to trains in tunnels, *Earthquake Engineering and Structural Dynamics* 21 (1992) 445–460.
[5] X. Sheng, C.J.C. Jones, D.J. Thompson. A discrete wavenumber coupled finite and boundary element model from ground vibration from tunnels, in: *Proceedings of the Eighth International Conference on Recent Advances in Structural Dynamics*, July 2003.
[6] P. Chatterjee, G. De Grande, D. Clouteau, T. Al-Hussaini, M. Arnst, R. Othman, Numerical modelling of ground borne vibrations from underground railway traffic, Report of the CONVURT Project, 2003.
[7] *Sprayed Concrete Linings* (*NATM*) *for Tunnels in Soft Ground: Design and Practice Guide*, Institution of Civil Engineers, London, 1996.
[8] M. Petyt, *Introduction to Finite Element Vibration Analysis*, Cambridge University Press, Cambridge, 1998.
[9] J. Domínguez, *Boundary Elements in Dynamics*, Computational Mechanics Publications, Southampton, 1993.
[10] A.A. Stamos, D.E. Beskos, Dynamic analysis of large 3-D underground structures by the BEM, *Earthquake Engineering and Structural Dynamics* 24 (1995) 917–934.
[11] M. Doblaré, L. Gracia, On non-linear transformation for the integration of weakly-singular and cauchy principal value integrals, *International Journal for Numerical Methods in Engineering* 40 (1997) 3325–3358.
[12] S. Ahmad, P.K. Banerjee, Multi-domain BEM for two-dimensional problems of elastodynamics, *International Journal of Numerical Methods in Engineering* 26 (1988) 891–911.
[13] C.J.C. Jones, D.J. Thompson, M. Petyt, Ground-borne vibration and noise from trains: elastodynamic analysis using the combined boundary element and finite element methods, ISVR Technical Memorandum 844, Institute of Sound and Vibration Research, University of Southampton, 1999.
[14] L. Andersen, C.J.C. Jones, Three-dimensional analysis using multiple boundary element domains, ISVR Technical Memorandum 867, Institute of Sound and Vibration Research, University of Southampton, 2002.
[15] A.T. Peplow, C.J.C. Jones, M. Petyt, Surface vibration over a layered elastic half-space with an inclusion, *Applied Acoustics* 56 (1999) 283–296.
[16] H. Takemia, K.-S. Shim, K. Goda. Embankment train track on soil stratum and wave impeding block (WIB) measured for vibration reduction, in: A.S. Çakmak, C.A. Brebbia (Eds.), *Soil Dynamics and Earthquake Engineering*, Vol. VII, Computational Mechanics Publications, Southampton, 1995, pp. 103–112.
[17] N. Chouw, G. Pflanz, Reduction of structural vibrations due to moving load, in: N. Chouw, G. Schmid (Eds.), *Wave 2000*, A.A. Balkema, Rotterdam, 2000, pp. 251–268.